PHYSICAL REVIEW B **84**, 052101 (2011)

Tunable helium bubble superlattice ordered by screw dislocation network

Zengfeng Di,[1,3,*] Xian-Ming Bai,[2] Qiangmin Wei,[1] Jonghan Won,[2] Richard G. Hoagland,[2] Yongqiang Wang,[2] Amit Misra,[1]
Blas P. Uberuaga,[2] and Michael Nastasi[1]
[1] *Materials Physics and Applications Division, MPA-CINT, Los Alamos National Laboratory, Los Alamos, New Mexico, 87545, USA*
[2] *Materials Science and Technology Division, MST-8, Los Alamos National Laboratory, Los Alamos, New Mexico, 87545, USA*
[3] *State Key Laboratory of Functional Materials for Informatics, Shanghai Institute of Microsystem and Information Technology, Chinese Academy of Sciences, Shanghai 200050, China*

(Received 24 May 2011; revised manuscript received 26 July 2011; published 24 August 2011)

Helium bubble nucleation at low-angle twist boundaries in gold has been investigated. It is found that the helium bubbles preferentially nucleate at screw dislocation nodal points and result in helium bubble superlattice formation, which is completely isomorphic with the screw dislocation network along the twist-grain boundary. Molecular statics calculations reveal that defect formation/solution energies along the screw dislocations, especially at the nodal points, are lower than their bulk counterparts. It is believed that this driving force is responsible for the helium bubble superlattice formation. Our study suggests that grain boundary engineering via adjustable twist angles in parallel boundaries to form tunable 3D bubble superlattices could afford a very promising approach for design of radiation tolerant materials.

DOI: 10.1103/PhysRevB.84.052101 PACS number(s): 61.72.Mm, 61.72.J−, 61.72.Lk, 61.50.Lt

The demand to reduce reliance on fossil fuels while meeting rapidly growing energy needs has renewed interest in nuclear energy—both fission and fusion. High energy particles in nuclear power environments induce displacements of large numbers of atoms in structural materials from their lattice positions, creating excess defects (vacancies and self-interstitial atoms) and generating insoluble helium from transmutation reactions. The combination of helium and defects leads to a microstructural evolution in which helium bubbles often form and contribute to both swelling and embrittlement, degrading the properties of fuel cladding and first-wall materials of nuclear reactors.[1,2] However, recent proposals have suggested that helium bubbles could be managed, thereby transforming them from a liability into an asset in controlling damage evolution in irradiated materials.[1,3] Odette and Hoelzer[1] propose that nanometer-scale helium bubbles can act as sinks for point defects, providing enhanced immunity to radiation damage. It has also been shown that interfaces, phase boundaries, and grain boundaries can mitigate radiation defects and influence helium bubble nucleation and growth.[4–8] In many cases this has been attributed to the presence of dislocations that make up the interface structure.[9–11]

Based on these previous findings it appears that the important consideration in helium management at interfaces is to understand the role of interface structure on helium bubble nucleation and growth. In this work we create well-defined grain boundaries in gold, i.e., pure twist boundaries, with precisely controlled twist angles forming a well-defined screw-dislocation network. We investigate the role of grain boundary structure on the nucleation and growth of helium bubbles. We observe that helium bubbles preferentially nucleate at the nodes of the screw dislocation network, forming a helium bubble superlattice. Molecular statics' calculations suggest that bubble formation is associated with lower vacancy formation energy and lower He-solution energies within the screw dislocations and dislocation nodes.

Single crystal (001) Au films, 50 nm in thickness, were deposited on 600-nm Ag single-crystal layers, which had been deposited on polished NaCl substrates by means of electron-beam evaporation. The deposition temperatures were set at 350 °C and 50 °C for Ag and Au, respectively, and the deposition rate was 2 Å/s. The 50 nm–50-nm Au-Au twist boundary was obtained by welding two Au/Ag/NaCl assemblies together with a 1° twist with respect to each other around their common normal, i.e., [001] orientation. After welding, the NaCl substrates were dissolved in water, and the Ag buffer layers were etched away by 20% HNO_3 solution. The remaining free-standing Au bicrystal specimen was placed on a copper grid and implanted at 250 °C with a fluence of 5×10^{15} cm^{-2} He ions at an energy of 22.5 keV. The implantation energy was chosen to ensure that all implanted He ions remained within the Au bicrystal and that the maximum concentration of implanted He coincided with the position of the twist boundary. The implantation temperature was chosen to assist in helium bubble formation and with consideration of the bubble-denuded zone as discussed later. For comparison, a 100-nm-thick single-crystal Au foil was subjected to an identical implantation. The samples before and after He implantation were examined without any additional sample thinning or ion milling with transmission electron microscopy (TEM) using a FEI Tecnai F30 operated at 300 kV.

As shown in Fig. 1, a square grid of screw dislocations with a periodicity of 15 nm is created along the bonding interface of the Au bicrystal. According to Frank's law,[12] the spacing between the screw dislocations, Λ, is related to the misorientation angle, Θ:

$$\Lambda = \frac{b}{2\sin(\Theta/2)} \tag{1}$$

where b is the Burgers vector ($b = a_{\mathrm{Au}}/2<110>$). Using $\Lambda = 15$ nm (as measured from our sample) and $b = 0.288$ nm, the corresponding misorientation angle is calculated as 1.1 degrees, which is close to the intended 1-degree misorientation angle.

Figure 2(a) illustrates the association between helium bubbles and the nodes of the screw dislocation grid. It is clear

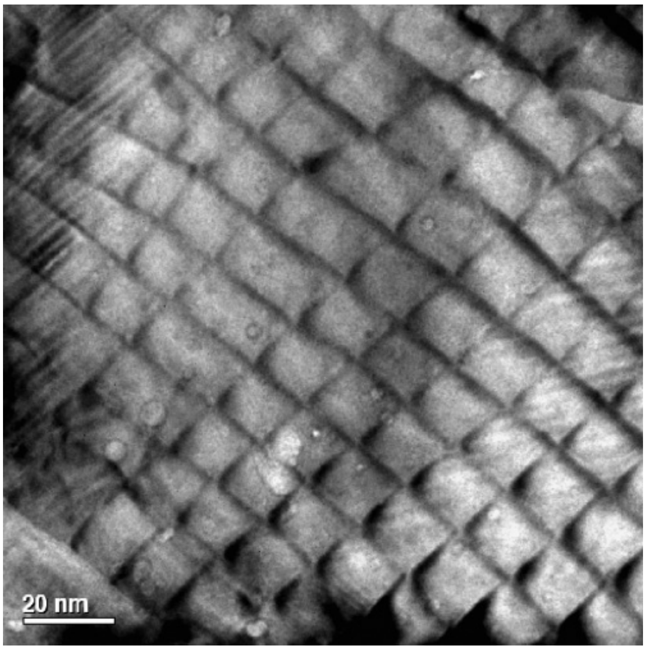

FIG. 1. A square network of screw dislocations in a (001) twist grain boundary with a misorientation angle $\Theta \approx 1^\circ$.

that helium bubbles are formed exactly at the nodal points of the dislocation network, while no detectable helium bubbles are observed in the matrix. By duplicating the symmetry and alignment of the dislocation network, all observable helium bubbles are assembled two-dimensionally into a bubble superlattice at the grain boundary plane with areal density of $6\times10^{11}\text{cm}^{-2}$. The sizes of the helium bubbles are relatively uniform with an average radius of about 1.2 nm. In comparison, as shown in Fig. 2(b), randomly distributed helium bubbles with an areal density of $2\times10^{12}\,\text{cm}^{-2}$ are formed in the single-crystal gold foil subjected to identical implantation conditions. The suppression of helium bubble formation in the Au bicrystal is believed to be correlated with the grain boundary. Similar as interfaces in nanolayered composites,[7] the grain boundary, which has large excess free volume and higher diffusivity of point defects, provides inexhaustible sinks for radiation-induced point defects and a catalyst for efficient Frenkel pair annihilation. Fewer vacancies residual in the Au bicrystal retard the helium bubble nucleation subsequently. TEM-focusing experiments and the size variation of helium bubbles suggest they are distributed at different depths throughout the pure Au foil; they are clearly larger than those that form at the nodes of the screw dislocation network. Comparison of Figs. 2(a) and 2(b) indicates that in the twist grain boundary (GB) all helium bubbles are formed at the same depth, i.e., the plane of twist grain boundary. Otherwise, the TEM image in Fig. 2(a) would show a similar random distribution of He bubbles as in the single-crystal case.

To understand the correlation between He bubble formation and the grain boundary structure, molecular statics were used to calculate the vacancy formation energy, E_{vac}, and the He substitutional and interstitial solution energies for various atomic sites in a model of a twist boundary. These calculations were performed on Cu, rather than Au, as Cu has the same face-centered cubic structure as Au and, more importantly, well-established interatomic potentials exist for the Cu-He system. We expect that our results on Cu give qualitative insight into the behavior in Au. Further, as we will show, calculation of vacancy behavior near twist boundaries in Cu shows very similar behavior in Au. In these calculations we used the embedded atom method potentials developed by Voter *et al.* for Cu-Cu[13] and by Wang *et al.* for Cu-He interactions.[14] The twist grain boundaries were created by rotating two perfect Cu crystals around their [100] axes, with (100) planes parallel to the formed boundary. The rotation angle between the two grains was 8.17°, chosen to reduce the model size. As the twist angle is still relatively small, resulting in a boundary structure that is still composed of an intersecting screw dislocation network, this boundary reproduces all of the essential features that would be present in the 1° boundary examined in the experiments. The resulting dimensions of the model were 5.07 nm × 5.07 nm × 2.89 nm, containing 6304 Cu atoms. Periodic boundary conditions were used in all directions. In order to find the minimum GB-energy structure, one grain was shifted relative to the other grain along a 21 × 21 point grid at

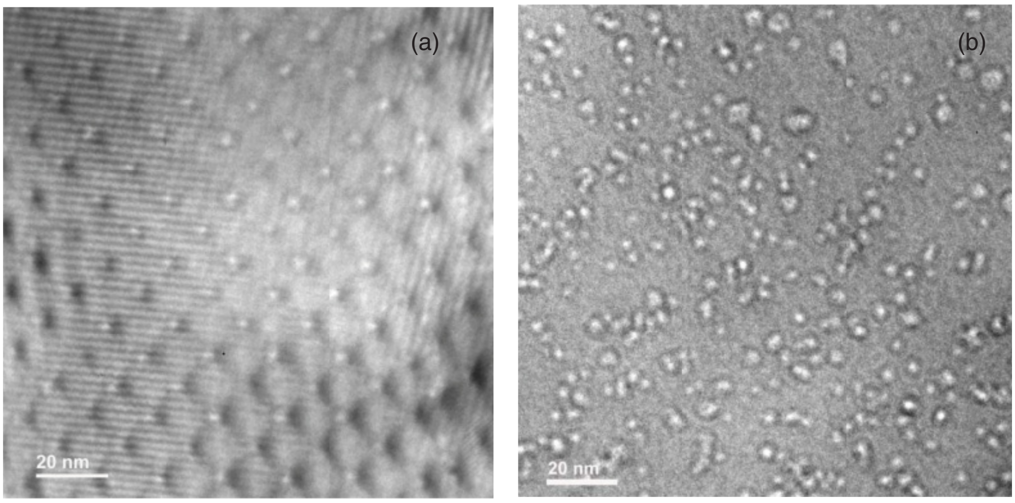

FIG. 2. Plan view of specimens with 22.5 keV $5 \times 10^{15}\text{cm}^{-2}$ He implantation at 250 °C: (a) Au bicrystal; (b) pure Au foil.

the grain boundary plane. At each point a conjugate gradient energy minimization method was used to minimize the GB structure. The GB structure used in subsequent calculations is the minimum-energy structure from this energy surface, i.e., gamma surface, mapping. The spacing between dislocations within the network is 1.79 nm, in agreement with Eq. (1) using $\Theta = 8.17^\circ$ and $b = 0.256$ nm. To calculate the vacancy formation energy as a function of position near the GB, every atom within the system was removed, one at a time, and the energy of the resulting structure was minimized. Figure 3(a) shows the formation energy of the vacancy near the twist GB, relative to the formation energy in perfect crystal Cu—a negative energy indicates a more favorable site for vacancy formation. Similarly, the relative solution energy of He as a substitutional species (replacing Cu atoms) and as an interstitial species were calculated, as shown in Fig. 3(b) and Fig. 3(c), respectively. Interstitial sites were identified by the method of Jiang *et al.*[15]

The results show the relation between the defect formation/solution energies and the structure of the twist boundary. In all cases the energies are lower at the cores of the screw dislocations than in regions away from the GB. Moreover, the energies are significantly lower within the nodes of the dislocation network. Near the center of each grid where the screw dislocation fields cancel, the vacancy and solution energies are nearly the same as perfect crystal values. Within

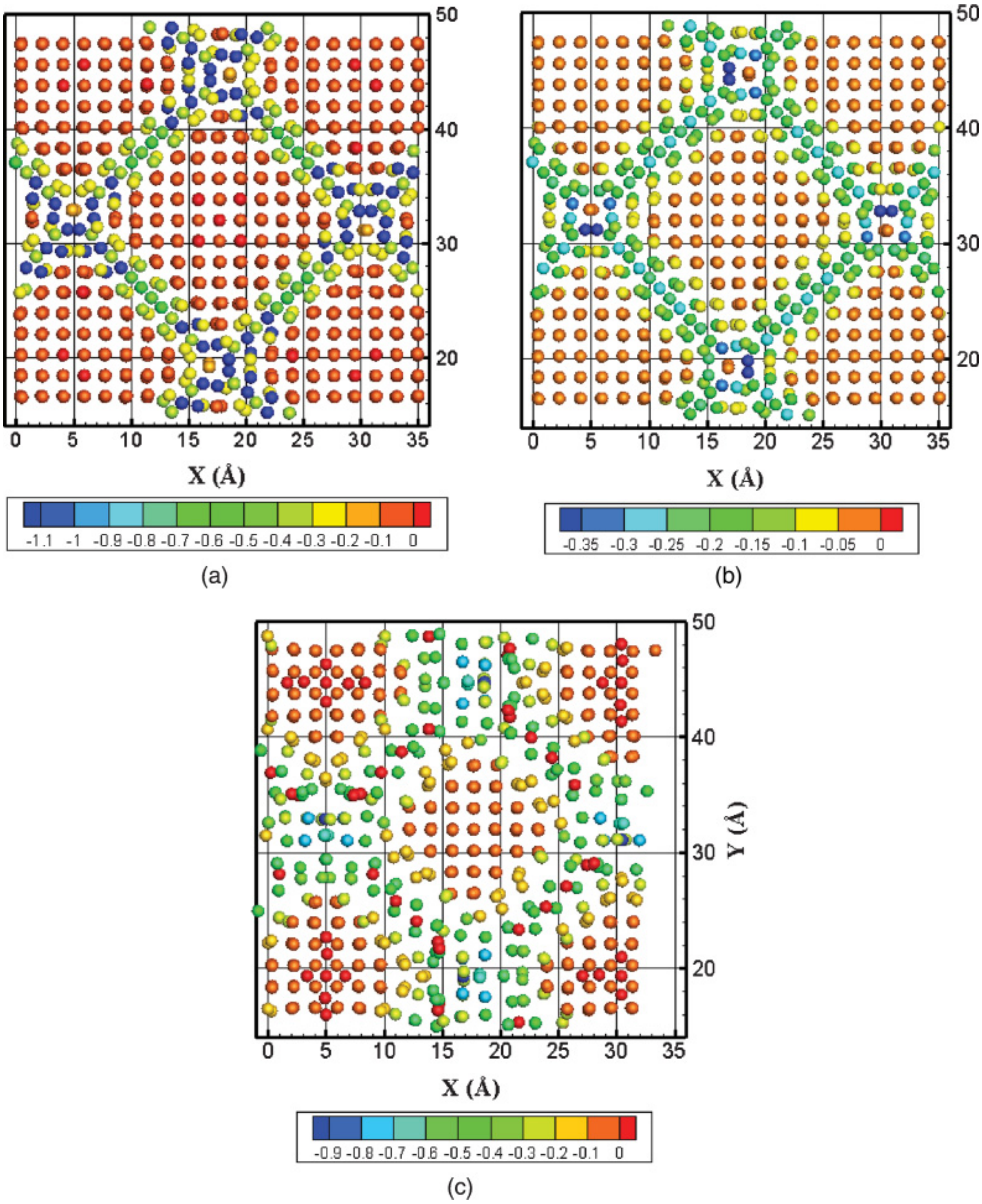

FIG. 3. (Color online) Formation and solution energies relative to the bulk for different atom sites along (001) 8.17° twist boundary of Cu bicrystal (a) pure Cu vacancy; (b) substitutional He; (c) interstitial He. Only a portion of the calculated twist GB plane is shown in each figure for clarity. The color of each defect site represents their respective defect formation energy. Note a value of zero in each figure represents the respective energy in the bulk region.

the nodal regions the vacancy formation energy is about 1.16 eV lower than the value in perfect Cu, 1.27 eV. Thus, the vacancy formation energy at nodal points is nearly zero indicating that vacancies can easily form at the nodes. This extremely low-vacancy formation energy at the intersection point of two screw dislocations is consistent with the calculations by Nomura *et al.*[16] The vacancy-formation energy within the core of a screw dislocation is about 0.6 eV lower than the bulk value. The decrease in formation energy of the vacancy implies a lower He diffusion activation energy E_a when diffusion is via a vacancy mechanism, since E_a is the sum of the migration energy and the formation energy of the mediating defect. In this case the migration energy of the vacancy is either unchanged or lowered near the boundary. Similar calculations on a twist boundary in Au find very similar behavior: the vacancy formation energy at the nodes is 0.97 eV lower than the bulk value, while it is about 0.46 eV lower at the screw dislocation cores. This gives us confidence that the calculations on Cu are representative of the behavior in Au.

Consistent with our calculations, dimer calculations in alpha-iron indicate that vacancies lower their energy by moving toward a screw dislocation where they become strongly trapped.[17] Once trapped in the core region of the screw dislocation, the vacancy can migrate along the dislocation line with a lower migration energy until it interacts with another defect such as with He or other vacancies; the migration energy of a vacancy along the core of a screw dislocation in alpha-iron was found to be about half of that in the bulk.[17] These results along with the information presented in Fig. 3(a) suggest that the clustering of vacancies will be highly probable along the screw dislocations and even more so at the intersections, leading to the formation of bubbles, which are comprised of vacancy clusters and helium atoms.

Helium bubble formation, as shown in Fig. 2(a), requires an agglomeration of He at nodal points. Helium diffusion could occur via either a vacancy (the dominant mechanism at equilibrium) or interstitial (possibly transiently during irradiation) mechanisms. Therefore, we investigate the solution energies of both substitutional and interstitial He to see whether the dislocation network induces He segregation. The relative solution energy of substitutional He near the twist GB is shown in Fig. 3(b), revealing a pattern that is similar to that of the vacancy [Fig. 3(a)], although the magnitude of the segregation energy is much smaller. The formation energy of substitutional He is lower in the cores of the screw dislocations and lowest at the nodal points compared to the perfect crystal. The maximum reduction in the substitutional He-solution energy is about 0.38 eV at the nodal points of the screw dislocation network, while it is about 1.16 eV for vacancy formation. As the structure of He interstitials is more complex than substitutional He, the interstitial He-solution energy map [Fig. 3(c)] does not precisely mirror the atomic structure of the grain boundary but still exhibits the general features of the screw dislocation network. As with the other defects, the interstitial He-solution energies are lower at sites near the screw dislocation cores and nodal points than in the interior regions of the grids. The minimum formation energy of interstitial He is at the nodal region and is 0.92 eV lower than in perfect crystal.

The data in Fig. 3 suggest that: (1) vacancies have an energetic preference to reside in the screw dislocation lines and nodes, particularly at the nodal points; and (2) regardless of the form it adopts (interstitial or substitutional), He also prefers to reside at the nodal points in the dislocation network. Thus, there are thermodynamic driving forces for He to be at the nodal points, which favors these as nucleation sites for He bubbles.

Nanostructured ferritic alloys (NFAs) have received a great deal of attention because of their excellent mechanical properties and resistance to irradiation damage. NFAs are Fe alloys with nanometer-sized oxide particles dispersed in the matrix. Recently, it has been proposed that one reason NFAs exhibit such high radiation tolerance is due to the formation of dispersed He bubbles at the interfaces between the oxide particles and the matrix. Normally, He is viewed as a liability, as the formation of He bubbles that grow without bound lead to swelling of the material. In NFAs the high density of oxide particles results in a high density of nanometer-sized He bubbles. These dispersed bubbles are excellent sinks, not only for He, but irradiation-induced defects (interstitials and vacancies) because they act nearly like a perfect surface. As a result, NFAs transform He from a liability to an asset, increasing the radiation tolerance of the material.[1,3]

In the present work we also obtain a large concentration of nanometer-sized He bubbles, formed on the intersections of the screw dislocation network of the twist boundary. Thus, by changing the twist angle, one can control the density of He bubbles and thus the overall radiation tolerance of the material. Clearly, in a real material, one twist boundary is not going to provide a sufficient density of He bubbles, but if a three-dimensional dislocation network can be built into the material, a high density of dispersed He bubbles could be achieved even in a single component material such as Au, again transforming He from a liability to an asset and providing enhanced radiation tolerance.

To ensure the maximal capture of He into the nodes of the dislocation network, the spacing between those nodes

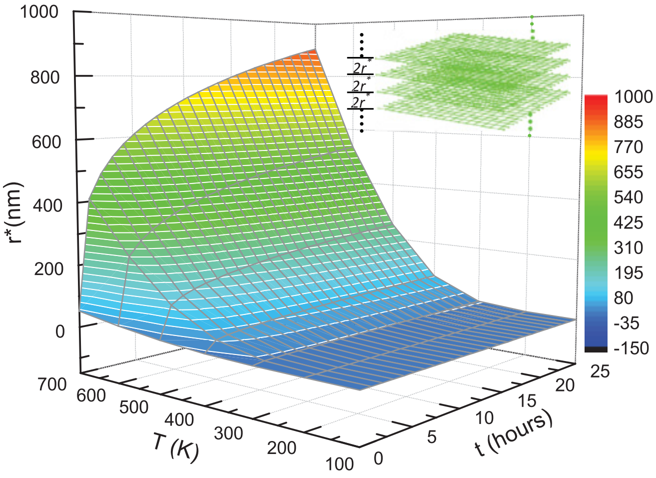

FIG. 4. (Color online) The radius of bubble-denuded zone for twist grain boundary in gold vs irradiation temperature and irradiation time. The proposed three-dimensional screw dislocation network is inserted as well.

must be controlled. That means that the spacing must be smaller than twice the width of the bubble-denuded zones often observed near boundaries in irradiated materials.[10] If the distance between nodes within the three-dimensional network is smaller than the He-node interaction distance, all He will eventually become trapped at nodes. Using the relationship proposed by Weeks *et al.*,[18] the width of the bubble-denuded zone can be estimated as

$$r^* = \left[\frac{20}{\pi^2}\frac{D_v}{kT}\Omega G b^2\left(\frac{1-v}{7-5v}\right)t\right]^{\frac{1}{4}} \tag{2}$$

$$D_v = D_0 \exp\left(-\frac{E_a}{kT}\right), \tag{3}$$

where D_v is the volume diffusion coefficient, D_0 is the pre-exponential coefficient, E_a is the activation energy for diffusion, k is Boltzmann's constant, T is absolute temperature of helium implantation, Ω is the atomic volume, G is the shear modulus of the matrix, b is the Burger's vector of the screw dislocation, ν is Poisson's ratio, and t is the implantation duration, respectively. Using values corresponding to the Au system ($D_0 = 0.091\ \mathrm{cm}^2/\mathrm{s}$;[19] $E_a = 0.82\ \mathrm{eV}$;[19] $k = 1.38 \times 10^{-23}\,\mathrm{J/K}$; $\Omega = 1.18\times10^{-23}\mathrm{cm}^3$; $G = 27$ Gpa; $b = 2.88\times10^{-8}$cm; and $\nu = 0.42$), the radius of the bubble-denuded zone for the twist grain boundary is plotted against irradiation temperature and irradiation time in Fig. 4. In general, the bubble-denuded zone increases with increasing irradiation temperature and irradiation time. At low temperature where vacancies, and thus He, are relatively immobile, the bubble-denuded zone is barely observed. However, it rapidly increases at high temperature. The twist grain boundary could even attract vacancies or helium a half micron away when the irradiation temperature is 700 K. Using values consistent with our experimental conditions, i.e., $T = 523$ K and $t = 1$ h, we calculate $r^* = 140$ nm, which is close to experimentally observed denuded zones (∼100 nm) in Al at similar homologous temperatures.[20] In a material in which a three-dimensional node network is formed from layered twist boundaries, the spacing between those boundaries must be no greater than $2r^*$, as demonstrated in the insert of Fig. 4. Such architecture of twist boundaries may be promising for the design of radiation tolerant materials.

In conclusion we observe preferential helium bubble formation at the nodes of screw dislocations formed along a twist boundary in Au. The screw dislocation network provides a perfect template for helium bubble formation, resulting in a superlattice of helium bubbles coincident with the nodal structure of the dislocation network. Molecular statics calculations indicate that lower vacancy formation, substitutional He and interstitial He solution energies along the screw dislocations provide the driving force for the segregation of vacancies and helium atoms towards the screw dislocation, thus resulting in He bubble nucleation at dislocation nodes to form the bubble superlattice.

The experimental portion of this work was sponsored by the Laboratory Directed Research and Development (LDRD) program at Los Alamos National Laboratory under Project No. 20090061DR. The modeling work was supported as part of the Center for Materials at Irradiation and Mechanical Extremes, an Energy Frontier Research Center funded by the US Department of Energy, Office of Science, Office of Basic Energy Sciences under Award Number 2008LANL1026.

---

[*] Corresponding author: dizengfeng@hotmail.com

[1] G. R. Odette and D. T. Hoelzer, JOM **62**, 84 (2010).

[2] S. J. Zinkle and J. T. Busby, Materials Today **12**, 12 (2009).

[3] G. R. Odette, M. J. Alinger, and B. D. Wirth, Annu. Rev. Mater. Res. **38**, 471 (2008).

[4] M. J. Demkowicz, R. G. Hoagland, and J. P. Hirth, Phys. Rev. Lett. **100**, 136102 (2008).

[5] A. Misra, M. J. Demkowicz, X. Zhang, and R. G. Hoagland, JOM **59**, 62 (2007).

[6] N. Nita, R. Schaeublin, and M. Victoria, J. Nucl. Mater. **329–333**, 953 (2004).

[7] T. Shen, S. Feng, M. Tang, J. Valdez, Y. Wang, and K. Sickafus, Appl. Phys. Lett. **90**, 263115 (2007).

[8] X.-M. Bai, A. F. Voter, R. G. Hoagland, M. Nastasi, and B. P. Uberuaga, Science **327**, 1631 (2010).

[9] G. W. Greenwood, A. J. E. Foreman, and D. E. Rimmer, J. Nucl. Mater. **4**, 305 (1959).

[10] P. L. Lane and P. J. Goodhew, Phil. Mag. A **48**, 965 (1983).

[11] B. N. Singh, T. Leffers, W. V. Green, and M. Victoria, J. Nucl. Mater **125**, 287 (1984).

[12] F. C. Frank, Carnegie Institute of Technology Symposium on the Plastic Deformation of Crystalline Solids, Office of Naval Research **1**, 150 (1950).

[13] A. F. Voter, Los Alamos Unclassified Technical Report #LA-UR 93-3901 (1993).

[14] L. Wang and X. J. Ning, Chin. Phys. Lett. **20**, 1416 (2003).

[15] C. Jiang, S. A. Maloy, and S. G. Srinivasan, Scr. Mater. **58**, 739 (2008).

[16] M. Nomura and J. B. Adams, J. Mater. Res. **7**, 3202 (1992).

[17] H. L. Heinisch, F. Gao, and R. J. Kurtz, Philos Mag. **90**, 885 (2010).

[18] R. W. Weeks, S. R. Pati, M. F. Ashby, and P. Barrand, Acta. Metallurgica **17**, 1403 (1969).

[19] P. Shewmon, *Diffusion in Solids*, 2nd ed. (TMS Press, Warrendale, PA, 1989) p. 66.

[20] B. N. Singh, T. Leffers, W. V. Green, and M. Victoria, J. Nucl. Mater. **122**, 703 (1984).